10.21062/mft.2020.088  http://www.journalmt.com

# Microstructure of Zirconium Fuel Claddings: TEM and EBSD Studies of As-Received and Neutron-Irradiated Materials

Petra Gávelová[1], Patricie Halodová[1], Barbora Křivská[1], Cinthia Antunes Correa[1], Jakub Krejčí[2], Martin Ševeček[3,4], Vít Rosnecký[1]
[1]Research Centre Řež, s.r.o., Department of Material and Mechanical Properties, Hlavní 130, 250 68, Husinec-Řež, Czech Republic. E-mail: petra.gavelova@cvrez.cz, patricie.halodova@cvrez.cz, barbora.krivska@cvrez.cz, cinthia.correa@cvrez.cz vit.rosnecky@cvrez.cz
[2]UJP Praha a.s., Department of Alloys and Pseudoalloys, Nad Kamínkou 1345, 156 10 Prague, Czech Republic. E-mail: jakub.krejci@ujp.cz
[3]ALVEL, Opletalova 37, 110 00 Prague, Czech Republic. E-mail: martin.sevecek@alvel.eu

**Zirconium fuel claddings act as a first barrier against release of fission products during nuclear power plant operation and interim storage of the spent fuel. During the reactor operation, cladding tubes are exposed to different stress level at elevated temperatures and neutron irradiation in corrosive environment. It causes a material degradation by corrosion, cladding embrittlement by hydrides and radiation-induced damage or radiation growth and creep of the fuel rods. The irradiation damage effects mainly contribute to the loss of material ductility. In our study, microstructure of as-received (non-irradiated) Zr-alloys used in LWR (Zr1Nb, Zr-1Nb-1.2Sn-0.1Fe, Zr-1.5Sn-0.2Fe-0.1Cr) were examined by electron microscopy methods. Transmission electron microscope (TEM) was used to describe the microstructure of claddings used in different reactor conditions and identify the radiation-induced damage, which is presented on Zr1Nb irradiated to one standard campaign in the VVER-1000 active zone. Following Electron Backscatter Diffraction (EBSD) method on transparent foils complements the TEM results in larger area, i. e. by grain size and orientation or analysis of local misorientation after irradiation. Radiation-induced damage was observed in Zr1Nb metallic matrix as <a> type dislocation loops, presence of radiation-induced precipitates or partial amorphization of the secondary phase particles. EBSD method showed no changes in crystallographic orientation, but a local increase of dislocation density can be affected by neutron irradiation.**

**Keywords:** Zirconium alloys, Light Water Reactors, Neutron irradiation, TEM, EBSD

## 1 Introduction

Open this template, delete all texts, put your text of article in this template or write text in this template, Cladding materials operating in Light Water Reactors (LWR) are exposed to elevated temperatures and moreover, to high neutron fluxes in corrosion environment. Thereby, mechanical stability of cladding tubes is always a critical issue during reactor operation, but also wet and dry spent fuel storage or postulated accidents. In Pressurized Water Reactors (PWR), the temperature of the claddings can reach from 280 up to 400°C at compressive hoop stress of about 40-80 MPa due to pressurised coolant up to ~16 MPa. It creates a highly corrosive medium under normal reactor operating conditions. While there are several corrosion resistant materials that provide mechanical stability in elevated-temperature environment, the basic operating principle of fission reactors limit the usage of these candidates [1]. The cladding tubes must have a low neutron capture cross-section known as neutron transparency and that prefers zirconium (Zr) alloys over the other potential cladding materials used in LWR [2]. A relatively large number of various Zr-alloys correspond to different operating conditions and they also try to eliminate the negative effects of reactor environment. The potential risk is stress-corrosion cracking at pellet-cladding interaction, which can be caused by combined effect of reactive fission products and a load of the expanding pellets [3]. The structural integrity of Zr-claddings can be also affected by hydride precipitation causing a mechanism called Delayed Hydride Cracking (DHC), which may cause the release of fission products into the primary coolant [4]. Moreover, dimensional changes of the fuel rods, are caused by several phenomena as stress-free irradiation growth caused by fast neutrons, hydriding or irradiation creep at high temperatures and stress [3]. All these effects cause a cladding material degradation and they are still deeply studied.

Radiation-induced damage (RID) has a major influence on cladding embrittlement compared to the effect of hydrides in the Zr-metallic matrix [5]. The main microstructural changes in the α-Zr matrix phase

(hexagonal lattice, *hcp*) include radiation-induced <*c*> type dislocation loops, which have the main influence on mechanical properties compared to the <*a*> type dislocations [6]. Beside the dislocation loops, the nano-scale radiation-induced precipitates can be observed [7, 8]. Moreover, the partial amorphization of secondary phase particles is often evaluated in the literature [8, 9]. Nano-scale gas-filled cavities or vacancy voids, which are often characterized in the stainless-steel reactor internals [10, 11, 12], can be also observed in the Zr-alloys.

Pressurized water reactors can be divided into two groups, so-called western (PWR) and eastern (VVER) types. Both groups differ in chemical composition of corrosion environment (reactor coolant) and cladding materials. Generally, from operational and experimental experience, Zr-based alloys containing niobium are more corrosion resistant. While niobium-containing Zr-alloys were used in WWER since the beginning (e.g. E110: Zr-1%Nb), in PWR there was a change from previous Zircaloy-4 (Zr-1.5Sn-0.2Fe-0.1Cr) to niobium-containing alloys (e.g. M5: Zr-1%Nb, ZIRLO: Zr-1%Sn-1%Nb0,1%Fe) [13]. Chemical composition of several Zr-alloys mainly used in LWR is shown in the Tab. 1, all the alloys contain also Al < 75 ppm, B and Cd < 0,5 ppm, Mg < 20 ppm, and Hf < 50 ppm. [14].

***Tab. 1*** *Chemical composition of Zr-alloys used in Light Water Reactors [12].*

| Element | Zirconium alloys (chemical composition in wt. %) | | | | |
|---|---|---|---|---|---|
| | **Zircaloy-2** | **Zircaloy-4** | **M5** | **E110** | **ZIRLO** |
| **Nb** | - | - | 0.8 – 1.2 | 1.0 | 0.9 - 1.1 |
| **Sn** | 1.2 - 1.7 | 1.2 - 1.7 | 0.01 | - | 0.9 - 1.0 |
| **Fe** | 0.07 - 0.2 | 0.18 - 0.24 | 0.03 | 0.05 | 0.1 |
| **Cr** | 0.05 - 0.15 | 0.07 - 0.13 | 0.015 | - | - |
| **Ni** | 0.03 - 0.08 | - | 0.007 | < 0.002 | - |
| **N** | < 0.008 | < 0.0025 | 0.005 | < 0.006 | < 0.0065 |
| **O** | 0.09 – 013 | 0.09 – 0.14 | 0.11 – 0.16 | < 0.1 | 0.9 - 0.13 |

In our contribution, microstructure of the as-received (non-irradiated and non-deformed) materials Zr1Nb, Zr-1Nb-1.2Sn-0.1Fe and Zr-1.5Sn-0.2Fe-0.1Cr were evaluated by Transmission (TEM) and Scanning Electron Microscopy (SEM) to present the typical microstructure of Zr-claddings used in different reactor conditions. Moreover, RID in Zr1Nb alloy irradiated to ~2,5 dpa in the VVER-1000 reactor core with prototypical temperature and neutron energy spectrum is introduced in the contribution compared to the as-received material. Detailed analysis on TEM were completed by Electron Backscatter Diffraction (EBSD) mapping within SEM providing the microstructure examination in larger area. The combination of TEM and EBSD techniques, both performed on transparent foils prepared for TEM from the cladding wall (Fig. 1), was optimized as the appropriate methodology for complex characterization of RID.

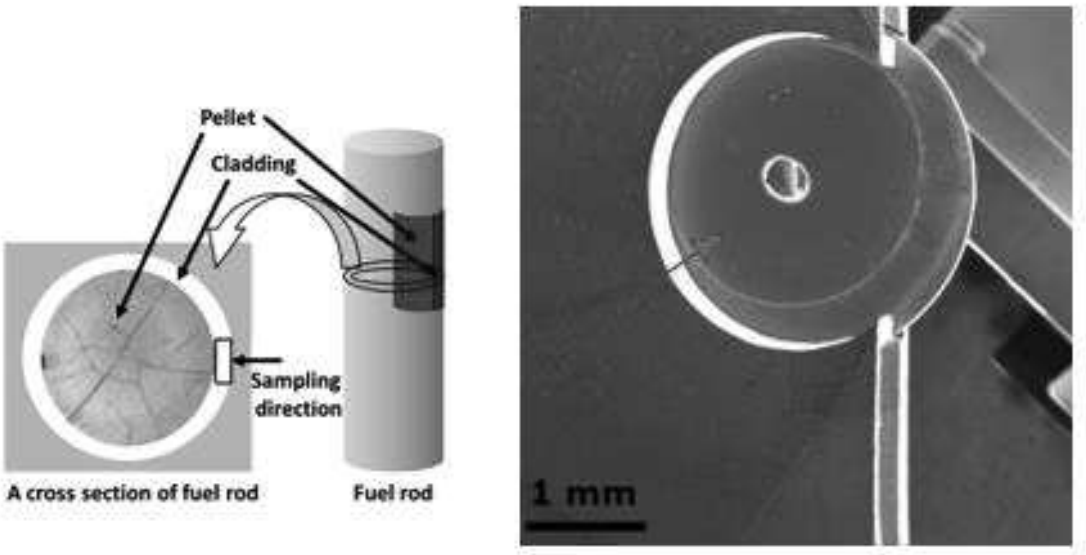


***Fig. 1*** *Cross-section of the fuel rod with indicated sampling (left image), transparent TEM foil in the SEM sample holder prepared for EBSD analysis (right image).*

## 2 Experimental

As-received cladding tubes Zr1Nb, Zr-1Nb-1.2Sn-0.1Fe and Zr-1.5Sn-0.2Fe-0.1Cr were evaluated by TEM and SEM methods. Transparent foils for electron microscopy were prepared from cladding wall by grinding on both sides to create a thin strip, from which Ø3 mm discs with thickness ~100 μm, were punched. Neutron-irradiated specimens were prepared in shielded hot-cells and glove box. Transparency of the foils was obtained by electrolytic polishing in 5% solution of perchloric acid in methanol with following conditions: temperature of electrolyte -65 °C, flow rate 4, voltage 30 V, electric current 10-12 mA. Thin foils were analysed by TEM JEOL JEM 2000FX ($LaB_6$) and 2200FS with accelerating voltage of 200 kV. TEM micrographs and phase identification were obtained using Bright Fied (BF) and Selected Area Electron Diffraction (SAED)/Nano Beam Diffraction (NBD) completed by Energy Dispersive Analysis (EDX). Size of secondary phase precipitates were evaluated using ImageJ, when the volume density was calculated as the number of precipitates in the examined area related to the conventional thickness of the foil 100 nm. Secondary phase precipitates in the neutron-irradiated Zr1Nb (Laves phases $Zr(Nb,Fe)_2$ and β-Nb) were evaluated using High Angle Annular Dark Field Detector (HAADF) in Scanning Transmission mode (STEM) to distinguish the areas with different chemical composition. In the case of irradiated material, BF imaging is not appropriate due to the high density of RID in the microstructure. Precipitates were observed in High Resolution mode (HR-TEM) and completed by STEM-EDX analysis.

For crystallographic (EBSD) analysis, FEG-SEM Lyra3 GMU for as-received and Mira3 GMU (Tescan) for neutron- irradiated specimen were used. EBSD was conducted after TEM analyses due to the carbon contamination of thin foils during EBSD mapping in SEM. The grain size distribution of α-Zr phase was evaluated from the area of 100 x 100 μm on EBSD maps in Euler angles. To identify the high angle grain boundaries, the critical parameter of misorientation for defining a grain was set to 15°. Then, the grain size was measured by fitted elipse. The analysis of local misorientation in grains known as Kernel Average Misorientation (KAM) can be calculated from EBSD maps to identify the areas with high dislocation density from slight orientation changes within individual grains. Then, the radiation defects (dislocation loops) as the cause of misorienation changes can be considered. As well, recrystallization of α-Zr grains was analysed owing to effect of neutron irradiation. The grains were distinguished on recrystallized (misorientation <1°), substructured (misorientation of subgrains >1°) and deformed fraction (mis. >1°and <15°) based on evaluation of misorientation inside the initial grains.

## 3 Results and discussion: Characterization of general microstructure of Zr-alloys using SEM-EBSD

SEM-EBSD analysis showed a different texture of the three as-received Zr-alloys operating in pressurized water reactors, as seen in the Fig. 2. Each Zr-alloy has a different texture, as a result of the distinct manufacturing process of the fuel rods. Zr1Nb is fully recrystallized (Recrystallized Annealed, RXA materials), while Zr-1Nb-1.2Sn-0.1Fe and Zr-1.5Sn-0.2Fe-0.1Cr alloys show only partial recrystallization (Stress Relieved Annealed, SRA materials) due to different heat treatment at the end of the manufacturing process.

Comparison of the as-received and neutron-irradiated Zr1Nb showed no change of crystallographic orientation, i. e. no recrystallization of α-Zr grains caused by interaction with fast neutrons was observed (Fig. 2, 3). Fig. 3 shows the increase of substructured grains in the neutron-irradiated Zr1Nb compared to the as-received material. It is due to the increase of the local misorientation inside of original α-Zr grains, caused by the presence of radiation-induced dislocations.

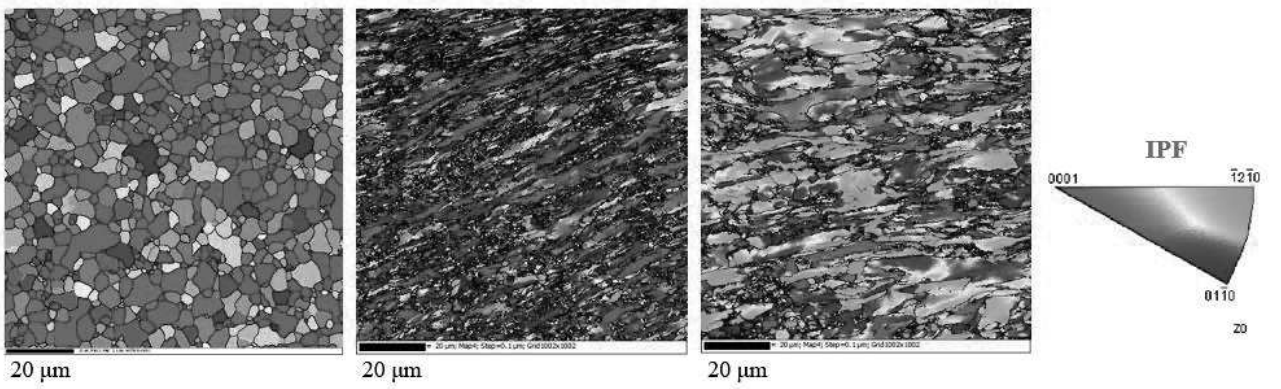


***Fig. 2*** *Inverse pole figure (IPFz) maps (100 × 100 μm) of as-received Zr-alloys (left image: Zr1Nb, middle image: Zr-1Nb-1.2Sn-0.1Fe, right image Zr-1.5Sn-0.2Fe-0.1Cr; crystallographic orientation of each grain shown in the IPFz color key in normal direction).*

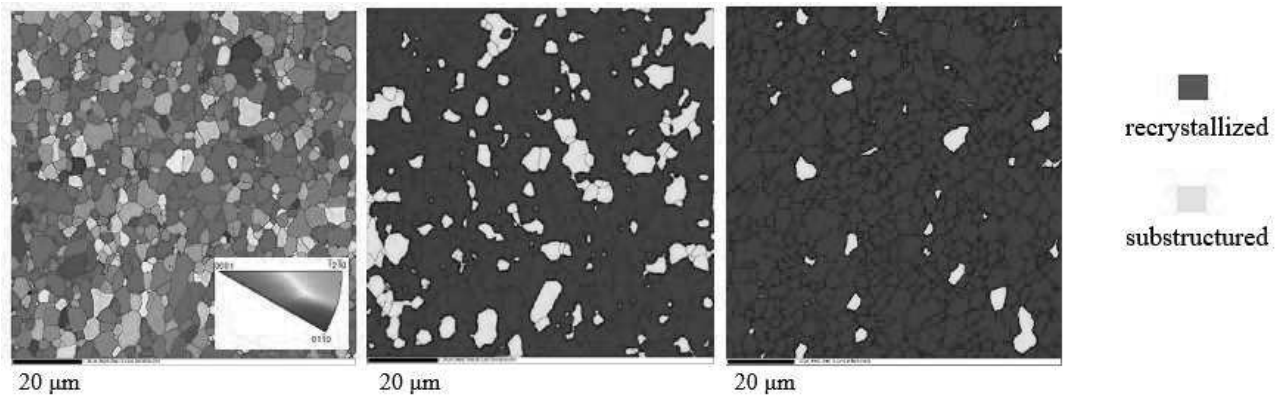


***Fig. 3*** *Left image: IPFz map (100 x 100 µm) of neutron-irradiated Zr1Nb, middle image: EBSD map of recrystallized fraction in irradiated Zr1Nb, right image: EBSD map of recrystallized fraction in the as-received Zr1Nb.*

Tab. 2 shows the average grain size of all analysed Zr-alloys and the recrystallized fraction in the as-received and neutron- irradiated Zr1Nb. The high scatter of values concerning Zr-1Nb-1.2Sn-0.1Fe and Zr-1.5Sn-0.2Fe-0.1Cr shows the strong texture of both cladding tubes presented in the previous Fig. 2. Grain size distribution of all specimens are shown in the following Fig. 4, where the distribution curves are similar for Zr-1Nb-1.2Sn-0.1Fe and Zr-1.5Sn-0.2Fe-0.1Cr as well as for the as-received and irradiated Zr1Nb.

***Tab. 2*** *Average grain size (AGS) of studied cladding materials and recrystallized fraction of as-received and neutron- irradiated Zr1Nb obtained from processing of EBSD maps.*

| Zr-alloy | Number of grains for AGS calculation [-] | Average grain size (AGS) [µm] | Recrystallized fraction [%] |
|---|---|---|---|
| **Zr-1Nb-1.2Sn-0.1Fe** | 7559 | 0.91 ± 0.79 | |
| **Zr-1.5Sn-0.2Fe-0.1Cr** | 3764 | 1.11 ± 1.21 | |
| **As-received Zr1Nb** | 893 | 2.97 ± 1.94 | 96 |
| **Neutron-irradiated Zr1Nb** | 900 | 3.02 ± 1.75 | 83 |

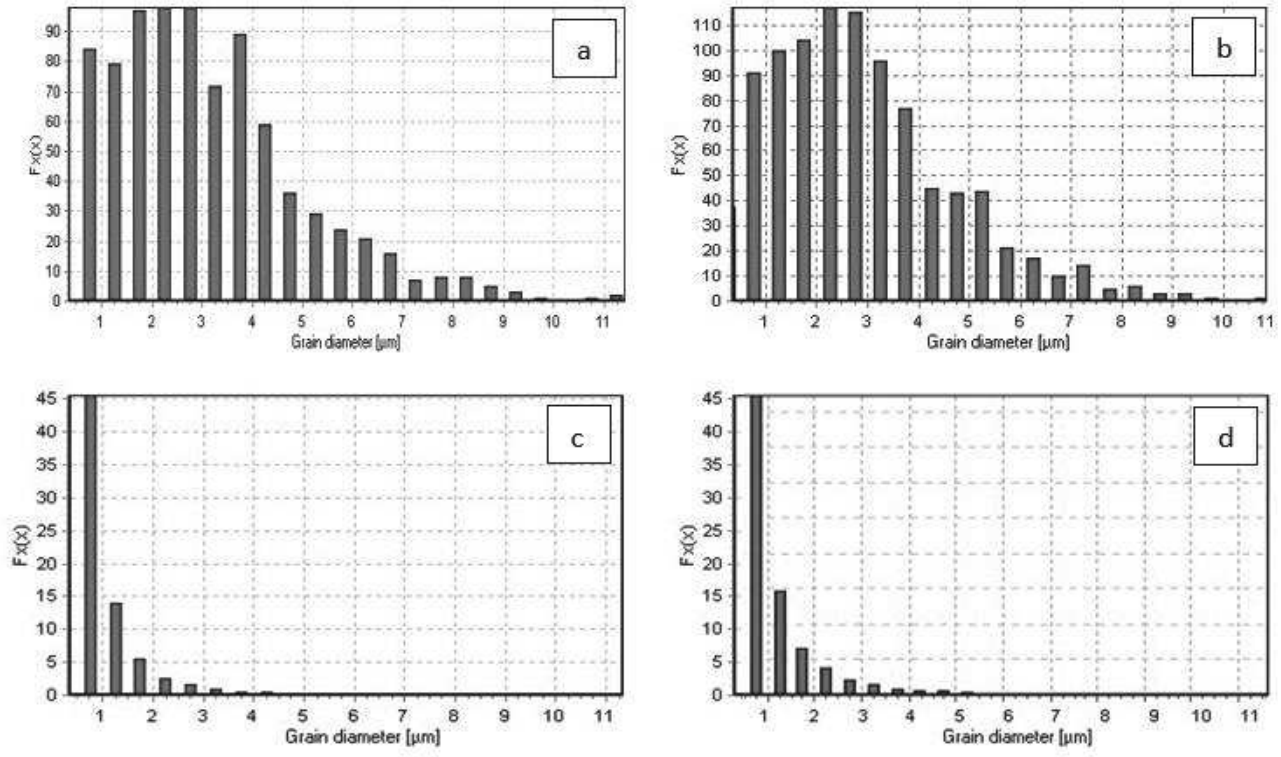


***Fig. 4*** *Grain size distribution of (a) as-received Zr1Nb, (b) neutron-irradiated Zr1Nb, (c) Zr-1Nb-1.2Sn-0.1Fe, (d) Zr-1.5Sn-0.2Fe-0.1Cr.*

Local misorientation analysis of Zr1Nb showed some areas with increased dislocation density in irradiated specimen compared to the as-received material, visible as the green regions in the Fig. 5. It is caused by the presence of radiation-induced defects (dislocation loops) in the α-Zr matrix phase. Low angle grain boundaries were observed in the as-received as well as irradiated specimen. For the both specimens, maximum of local misorientation (KAM value) is 0.35.

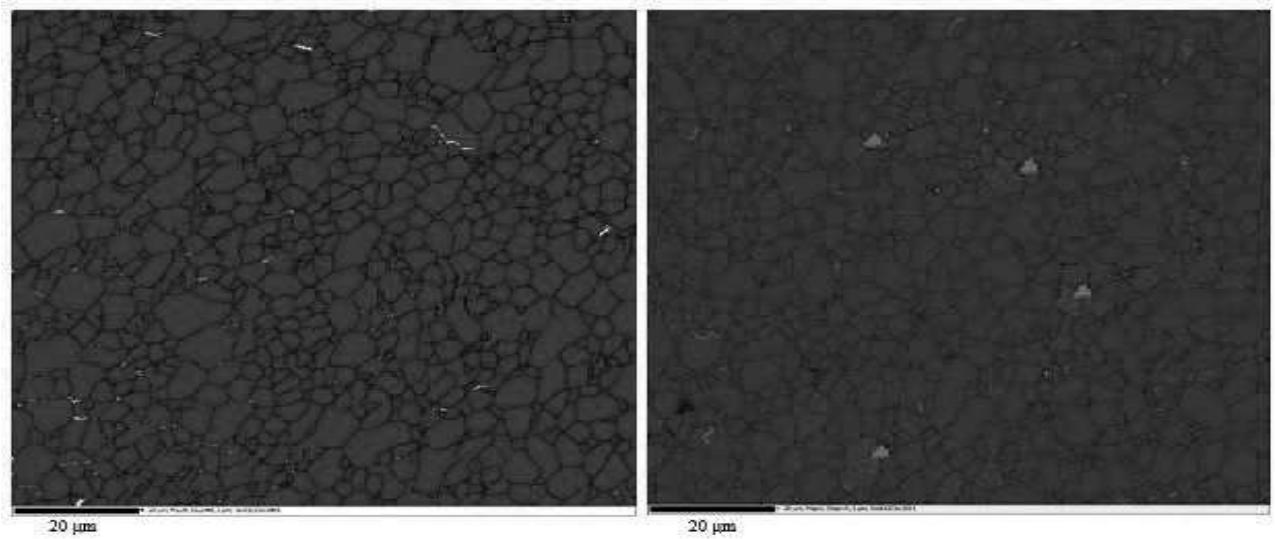


***Fig. 5*** *Local misorientation maps of the as-received (left image) and neutron-irradiated (right image) Zr1Nb with the filter 3x3 points. The areas with increased dislocation density indicated by green colour in maps and signed by red arrows.*

## 4 Results and discussion: Characterization of local microstructure of Zr-alloys using TEM

Following TEM analysis of the as-received specimens completed the EBSD results by detailed micrographs of the microstructure, identification of the secondary phase precipitates, volume density and the average size of precipitates. Fig. 6 shows the microstructure of the as-received Zr-alloys, i. e. overview micrographs (a-c) and some chosen details of the microstructure (d-f).

Zr1Nb (Fig. 6a) is characterized by polyhedral α-Zr grains with hexagonal (*hcp*) lattice containing secondary phase precipitates, i. e. Laves phases $Zr(Nb,Fe)_2$ with *hcp* lattice, Fig. 6d, and β-Nb particles with body-centered cubic (*bcc*) lattice. Precipitates with various size and shape are distributed inside α-grains as well as at the grain boundaries and have the average size of 43 ± 8 nm. Volume density of precipitates was calculated $1.1 \times 10^{20} \pm 3.8 \times 10^{19}$ $m^{-3}$. Dislocations were observed mostly inside the grains, in several places captured on precipitates.

Zr-1Nb-1.2Sn-0.1Fe (Fig. 6b, e) showed the elongated and deformed α-Zr grains with high dislocation density, the length of the grains was from hundreds of nanometers to units of micrometers. Deformed α-grains contain a dense dislocation network, which makes difficult the analysis of particles in the matrix. β-Nb particles, mainly globular, with the average size of 70 ± 20 nm were identified in the microstructure.

Zr-1.5Sn-0.2Fe-0.1Cr (Fig. 6c, f) contains deformed as well as recrystallized grains. Laves phases $Zr(Cr,Fe)_2$ were identified in the microstructure with the average size around 50 ± 35 nm. Volume density of precipitates was very low as in the case of Zr-1.5Sn-0.2Fe-0.1Cr, only a few particles were observed.

Radiation-induced damage in the neutron-irradiated Zr1Nb was observed in the α–Zr matrix phase, as seen in the Fig. 7 a-f. The irradiated Zr1Nb microstructure is characterized by polyhedral α–Zr grains with slightly rounded or straight high angle grain boundaries (Fig. 7a) as in the as-received material. The RID can be well-recognized in comparison with the non-irradiated state, where the α-Zr grain exhibit clear interior. The precipitates $Zr(Nb,Fe)_2$ and β-Nb are distributed in the α–Zr matrix visibly damaged by radiation defects observed as dark regions (Fig. 7b). Thereby, these precipitates were evaluated in STEM-HAADF mode to refine the volume calculations. The average size of precipitates was 62.5 ± 25 nm and the volume density were calculated $1.17 \times 10^{20} \pm 3.74 \times 10^{19}$ $m^{-3}$. Radiation-induced precipitates (probably β-Nb type) were observed in the α–Zr matrix with the size of units of nanometers (Fig. 7d). The primary precipitates of secondary phases were also affected by neutron irradiation, which was observed as the partial amorphisation of the precipitate/matrix boundary, as seen in the Fig. 7e. The presence of <*a*> type dislocation loops was observed. <*c*> type loops were not identified, however their presence in certain grains can be considered. Cavities were not found in the mictrostructure, probably due to the low neutron fluence.

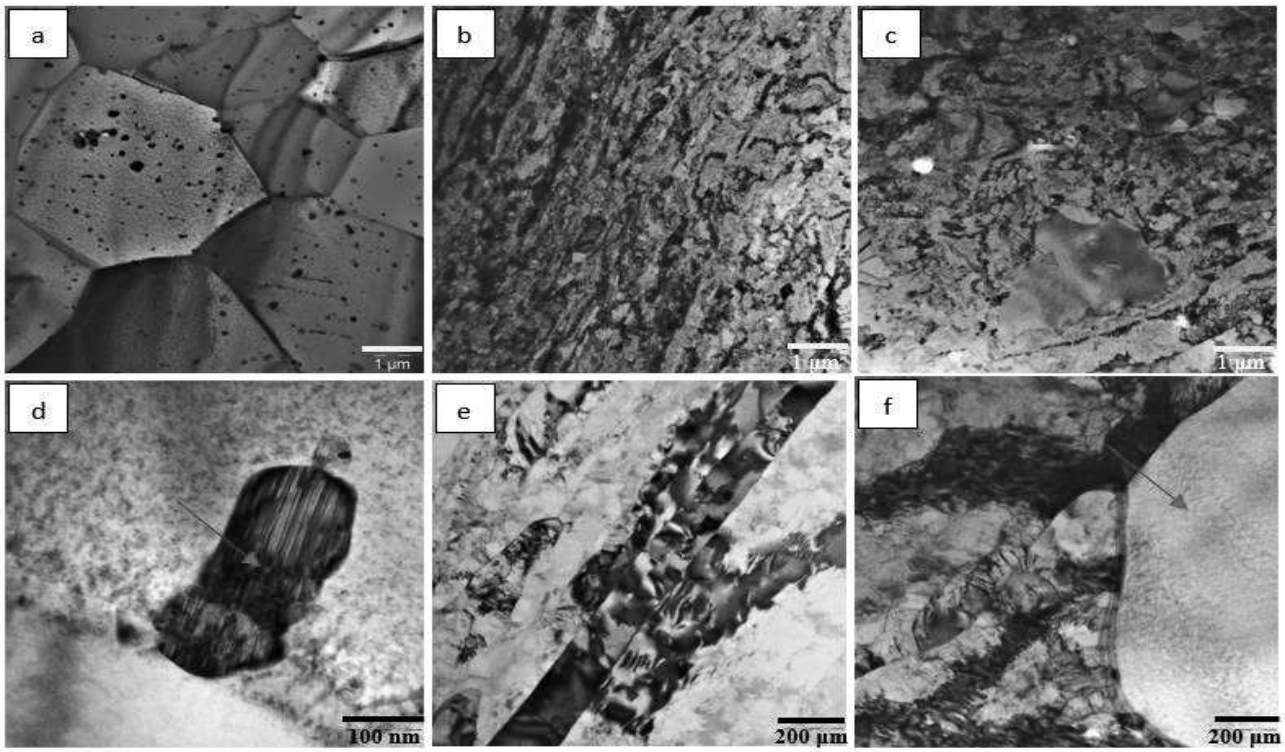


***Fig. 6*** *TEM-BF micrographs of the as-received Zr-alloys (a: Zr1Nb with amount of secondary phase precipitates in the polyhedral a-Zr grains, b: Zr-1Nb-1.2Sn-0.1Fe with elongated and deformed a-Zr grains, c: Zr-1.5Sn-0.2Fe-0.1Cr with deformed and recrystallized a-Zr grains-recrystallized grains signed by red arrows, d: Laves phase $Zr(Nb,Fe)_2$ in the Zr1Nb identified by SAED/EDX-signed by red arrow, e: detail of elongated a-Zr grains in the Zr-1Nb-1.2Sn-0.1Fe , f: boundary of recrystallized grain-signed by red arrow-and deformed grains of a-Zr phase in the Zr-1.5Sn-0.2Fe-0.1Cr).*

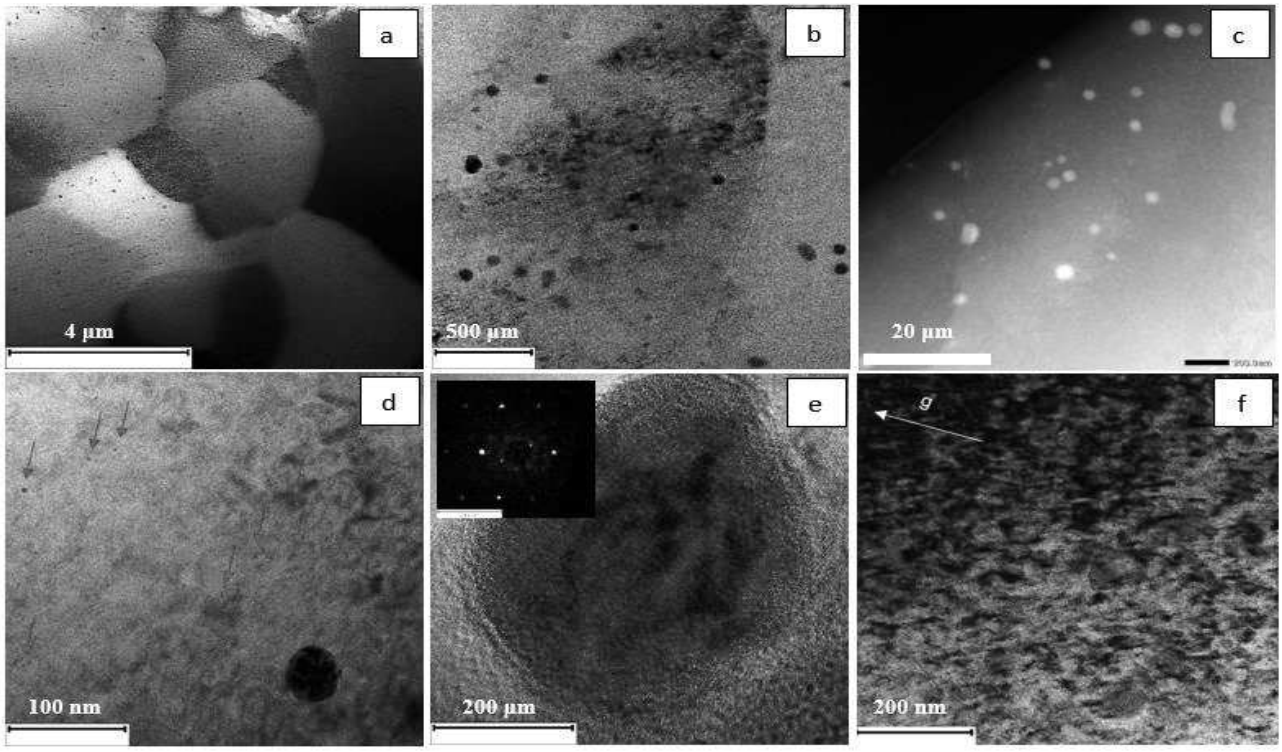


***Fig. 7*** *TEM micrographs of neutron-irradiated Zr1Nb (a: Overview micrograph with visible radiation damage – shown in diffraction contrast, b: The inner region of a–Zr matrix phase with globular precipitates and radiation damage observed as dark area, c: Precipitates imaged in STEM-HAADF mode for volume calculations, d: Radiation-induced precipitates in the matrix signed by red arrows, e: HR-TEM micrograph - partial amorphisation of β-Nb particle caused by neutron irradiation – NBD diffraction to confirm the presence of amorphous phase, f: <a> type dislocation loops imaged in BF close to the zone [0-111], diffracton vector g=[10-11].*

## 5 Conclusions

As-received cladding materials Zr1Nb, Zr-1Nb-1.2Sn-0.1Fe and Zr-1.5Sn-0.2Fe-0.1Cr were evaluated by Transmission and Scanning Electron Microscopy methods to present the typical microstructure of Zr-claddings used in different conditions of eastern and western types of pressurized water reactors. Both techniques used the transparent foils prepared for TEM.

Radiation-induced damage in Zr1Nb alloy irradiated to ~2,5 dpa in the VVER-1000 reactor core was evaluated compared to the as-received (non-irradiated) material.

Based on the results from EBSD mapping and TEM micrographs, the as-received Zr-alloys have a different texture due to a unique manufacturing process for each Zr-cladding material. Zr1Nb contains recrystallized α-Zr grains with average grain size of 2.97 ± 1.94 μm. Zr-1Nb-1.2Sn-0.1Fe and Zr-1.5Sn-0.2Fe-0.1Cr are partly recrystallized with average grain size of 0.91 ± 0.79 μm and 1.11 ± 1.21 μm, where the high scatter of values shows the strong texture with elongated and recrystallized grains. In the Zr1Nb microstructure, secondary phase precipitates $Zr(Nb,Fe)_2$ and β-Nb with the average size 43 ± 8 nm and volume density $1.1 \times 10^{20} \pm 3.8 \times 10^{19}$ $m^{-3}$ were evaluated. Due to the high dislocation density in deformed microstructure of Zr-1Nb-1.2Sn-0.1Fe and Zr-1.5Sn-0.2Fe-0.1Cr, only several particles, mainly in recrystallized grains, were observed. In the Zr-1Nb-1.2Sn-0.1Fe, β-Nb particles were indentified, while in the Zr-1.5Sn-0.2Fe-0.1Cr only Laves phases $Zr(Fe,Cr)_2$ were observed.

In the α–Zr matrix phase of neutron-irradiated Zr1Nb, radiation defects were observed as dark regions, where the secondary phase precipitates are distributed. The average size of precipitates was 62 ± 25 nm. The volume density was $1.17 \times 10^{20} \pm 3.74 \times 10^{19}$ $m^{-3}$, which is similar to the as-received Zr1Nb. From HR-STEM imaging, the amorphization of the precipitate/matrix boundary was observed as the effect of neutron irradiation. As well, nano-scale radiation-induced precipitates were recognized in the microstructure, probably of β-Nb type. Moreover, a presence of <*a*> type dislocation loops observed by TEM was confirmed by local misorientation analysis (EBSD), where a dislocation density in the irradiated specimen was increased compared to the as-received material. <*c*> type dislocation loops were not identified, however their presence in certain grains can be considered. As well, cavities were not observed in the mictrostructure of Zr1Nb.

## Acknowledgement

***Presented work was financially supported by the Ministry of Education, Youth and Sport Czech Republic - project LQ1603 Research for SUSEN. This work has been realized within the SUSEN Project (established in the framework of the European Regional Development Fund (ERDF) in project CZ.1.05/2.1.00/03.0108 and of the European Structural and Investment Funds (ESIF) in the project CZ.02.1.01/0.0/0.0/15_008/0000293) and Innovations for Competitiveness, Application - Call IV., CZ.01.1.02/0.0/0.0/17_107/0012555, 2017-2020.***

## References

[1] CENGEL Y. A., C. J. (2006). Fluid Mechanics: Fundamental and Applications, pp. 817-842. New York, USA

[2] NAMBURI, H., OTTAZZI, L., CHOCHOLOUSEK, M., KREJCI, J. (2018). Study of hydrogen embrittlement and determination of E110 fuel cladding mechanical properties by ring compression testing, 2018. In *International Conference on materials and Metallurgy*. 2018. ISBN: 978-80-87294-84-0.

[3] WEIDINGER, H. G. (2007). Zr-Alloys, the Nuclear Material for Water Reactor Fuel, In *7th International Conference on WWER Fuel Performance*, Albena, Bulgaria, 2007.

[4] IAEA: Delayed hydride cracking in zirconium alloys in pressure tube nuclear reactors. In *Final report of a coordinated research project 1998–2002. IAEA-TECDOC-1410.* Oct 2004.

[5] BLAT-YRIEIX, M., BOUFFIOUX, P. ET AL. (2017). Hydrogen pick-up in Zr-alloys. Phenomenology and impact on fuel assembly component behaviour. Lecture in Metallurgy and properties of Zr alloys for nuclear applications. Saclay. 2017.

[6] CHOI S.I., KIM E.H. (2013). Radiation-Induced Dislocation and Growth Behavior of Zirconium and Zirconium Alloys – A Review. In *Nuclear Engineering and Technology*, 45 (3), 385-392, 2013.

[7] V. N. SHISHOV, A. V. NIKULINA, V. A. MARKELOV, M. M., PEREGUD, A. V. KOZLOV, A. V. AVERIN, S. F. KOLBENKOV, A. E. NOVOSELOV. (1996). Influence of neutron irradiation on dislocation structure and phase compositin of Zr-base alloys. In *Zirconium in the Nuclear Industry: 11th Int. Symp.*, Garmisch-Partenkirchen, Germany, Sept. 11–14, 1995, ASTM STP 1295, p. 603, 1996.

[8] LIU, J., HE, G., CALLOW, A., LI, K., LOZANO-PEREZ, S., WILKINSON, A.,

MOODY, M., GROVENOR, CH., HU, J., KIRK, M., LI, M., HAQ MIR, A., HINKS, J., DONELLY, S., PARTEZANA, J., NORDIN, H. Ex-situ and In-situ Studies of Radiation Damage Mechanisms in Zr-Nb Alloys. In *ASTM 19th Symposium on Zirconium in the Nuclear Industry*.

[9] GRIFFITHS, M.; GILBERT, R. W.; CARPENTER, G. J. C. J. In *Nucl. Mater*. 1987, 150(1), 53–66.

[10] HOJNÁ, A. (2020). Overview of Intergranular Fracture of Neutron Irradiated Austenitic Stainless Steels. *Metals* [online]. 2017, [cited 2020-08-17]. Available from: http://www.mdpi.com/journal/metals/special_issues/radiation_effects. ISSN 2075-4701.

[11] BUBLÍKOVÁ, P., HALODOVÁ, P., FOKT, M., NAMBURI, H., ROSNECKÝ, V., PROCHÁZKA, J., DUCHOŇ, J., VOJTĚCH, D. (2018). Neutron irradiated reactor internals: An applied methodology for specimen preparation and post irradiation examination by electron microscopy methods. *Manufacturing technology* 2018. 18 (4), p. 545 – 551.

[12] VACKOVÁ, M., VALKO, M., PAVLENKO, S., HALKO, J. (2017). Methodology of increasing safety of welding joints in pressure vessels X5CrNi18-10. *Manufacturing Technology* 2017. 17 (4). p. 611-617.

[13] KREJČÍ, J. (2018). Oxidace palivového pokrytí v tepelně-chemických podmínkách jaderného reaktoru. *Disertační práce*. České Vysoké Učení Technické v Praze. Fakulta Jaderná a Fyzikálně Inženýrská. Praha, 2018.

[14] BANERJEE, S. (2001). Nuclear Applocations: Zirconium Alloys, Encyclopedia of Materials: Science and Technology (Second Edition) 2001, Pages 6287-6299, https://doi.org/10.1016/B0-08-043152-6/01117-7.